P-ISSN 2586-9000
E-ISSN 2586-9027
Homepage : https://tci-thaijo.org/index.php/SciTechAsia
Science & Technology Asia
Vol.27 No.3 July - September 2022
Page: [186-203]
*Original research article*

# 3D Numerical Analysis of Focused Microwave Ablation for the Treatment of Patients with Localized Liver Cancer embedded with a Vertical and Horizontal Blood Vessel

Wutipong Preechaphonkul, Phadungsak Rattanadecho*

*Center of Excellence in Electromagnetic Energy Utilization in Engineering, Department of Mechanical Engineering, Faculty of Engineering, Thammasat University, Pathum Thani 12120, Thailand*

Received 20 February 2021; Received in revised form 12 May 2021
Accepted 20 May 2021; Available online 29 September 2022

**ABSTRACT**

Microwave ablation (MWA) is the minimally invasive treatment technique. In this treatment, the microwave energy is transmitted by the microwave antenna into the un-wanted tissue (tumor). The microwave energy would be absorbed and converted to volumetric heat generated in tissue. The achievement of MWA is related to the temperature distribution in the treatment area. Tumors are usually located near the large blood vessels, and the heat convection by blood flow may affect the heat transfer in the treatment area. The modeling for heat transport in the biological tissue was applied in the therapeutics application to prevent injury and analyze the treatment process effectiveness. The present study presents the three-dimensional (3D) heat transfer in the liver cancer embedded with a single blood vessel during the MWA treatment model. The characteristic of a single vessel located between the horizontal vessel and vertical vessel was investigated on the SAR, temperature, and damaged tissue distribution. The mathematical model is considered, coupled with electromagnetic wave propagation, heat transfer, and blood flow in a large vessel analysis. The coupled nonlinear set of these equations is solved using the 3D finite element method (FEM). The results demonstrate the temperature distribution at the tumor boundary of the model embedded with a horizontal vessel was higher than the model embedded with a vertical vessel. The simulation results show the asymmetry of the temperature distribution, which emphasizes the necessity of 3D assumption. The value of investigated provided an indication of limitations that must be considered in administering microwave ablation therapy.

**Keywords:** 3D numerical modeling; FEM; Heat transfer; Liver cancer; Microwave ablation

***Corresponding author:** ratphadu@engr.tu.ac.th
**doi:** 10.14456/scitechasia.2022.55

## 1. Introduction

Microwave Ablation (MWA) is the minimally invasive and effective treatment method for liver cancer therapy [1, 2]. This treatment applies the microwave energy into the local cancer area (tumor) using the microwave antenna. The microwave energy is absorbed and converted to the internal heat generation [3]. The temperature of the tumor is increasing during this process. When tissue temperature rises above 52ºC, the cancer cell would immediately die [4-8]. This treatment aims to elevate the tumor temperature above 52 ºC where the tumor is destroyed and without damage to the surrounding tissue [9]. Therefore, understanding the heat transport mechanism in the treatment area is essential for treatment.

MWA has remarkably developed, showing the many advantages of this treatment over the surgical method [10]. The clear advantages of MWA treatment are minimal invasiveness and rapid treatment [11]. Although MWA is an exciting and effective treatment method, experimentation on humans' livers could not be conducted for both humane and ethical reasons. Some researchers have been experimenting with animals [10-13]. However, these experimental studies had limitations compared to experimenting with a nearly natural human liver. The numerical simulation could be applied to study the treatment. It has the advantage of needing only a short period, low cost, humaneness, and could be set up with conditions near to those of a real human liver [9].

Several years ago, many researchers developed mathematical models for predicting the temperature distribution in biological tissue. The most widely model was introduced by Pennes, which has become well known as the bioheat model [14]. The bioheat model is developed based on heat diffusion between biological tissue and blood vessels. Due to the Pennes bioheat simplification, many studies have established and developed the mathematics of extending and modifying the Pennes bioheat [15-17]. Moreover, some researchers investigated the effect of heat transfer between arteries, veins, and surrounding tissue [18-20]. The previous bioheat mathematical modeling studies were the critical foundation for developing the heat transfer in the biological tissue model during the MWA process.

In 2007, Yang et al. proposed the modified bioheat for MWA treatment and comparative with their experimental [21]. Yang et al. added the liver evaporation term to the original bioheat equation, and their model was the suitable predicting model in the high- temperature zone. However, the modified bioheat model by Yang et al. was not an accurately predicting model, which was proved by Keangin et al. [3]. Keangin et al. investigated the thermal expansion of liver cancer treatment with MWA by using numerical simulation. As a result, the deformation analysis model was much more accurate than the model without deformation analysis. Later, Wu et al. investigated the effect of multi- frequency on the liver cancer treatment model with MWA using numerical simulation [22]. Results showed that the high frequencies of microwaves significantly affected the heating pattern in the liver cancer model. In 2019, Xu et al. presented a large and round ablation zone using the tri-slot coaxial antenna for MWA treatment. Their study focused on the optimal design of the antenna via the finite element method (FEM) [23]. In 2020, Soltani et al. presented the effects of magnetic nanoparticle diffusion during the MWA treatment via a numerical approach [24].

Furthermore, the porous media theory was developed to be an approach for heat transfer analysis in biological tissue [25-30]. The benefit of the porous media approach is that it requires fewer assumptions than the bioheat approach [27]. However, the previous studies investigated the heat transfer under the two-dimensional (2D) and 2D axisymmetric assumption. The benefits of this assumption are faster calculation and

reduced complexity of the problem. However, the limitation of this assumption is that it cannot apply in an asymmetric treatment area, such as the treatment area near a large blood vessel.

Previously, the studies of heat transfer in the biological tissue during thermal treatment under the three-dimensional (3D) assumption have appeared. In 2015, Zorbas and Samaras investigated the effect of diameter and distancing of a single vessel on the cancer treatment model with radiofrequency ablation (RFA) [31]. After that, Shao et al. investigated the effect of nanoparticle injection on the liver cancer nearly countercurrent vessels during RFA treatment [32]. The simulation result was validated by their experiments, and the results represented the heat transfer in the liver tissue that nearby countercurrent vessels were an asymmetrical phenomenon. In 2018, Nabaei and Karimi proposed heat transfer in tumor treatment during the cryosurgery process and adjacent with the large blood vessel [2]. Moreover, Gheflati and Naghavi proposed the tumor treatment by using laser-induced hyperthermia embedded countercurrent vessels with the computational study [41]. Although the studies of heat transfer in the biological tissue during thermal treatment under the 3D assumption have appeared, the 3D studies of heat transfer in the biological tissue during MWA have rarely appeared. In addition, MWA treatment involves high temperature, and heat transfer is the essential key to the treatment. Moreover, the liver is one of the organs most involved in the complex vascular system that includes small, medium, and large vessels. Furthermore, when the potential heat transfer occurs near the large blood vessels, previous studies indicate that 3D assumption should analyze the problem.

The present study presents the 3D heat transfer in the liver cancer embedded with a single blood vessel during the MWA treatment model. The characteristic of a single vessel located between the horizontal vessel and vertical vessel was investigated. The mathematical model is considered coupled with electromagnetic wave propagation, heat transfer, and blood flow in a large vessel. The mathematical models were solved by using the finite element method (FEM) based on the 3D assumption. The characteristic of the vessel location was investigated on the SAR distribution, the temperature distribution, velocity profile, and the necrotic of damaged tissue in the 3D liver cancer treatment model. The results in this study can be used as a guideline for practical study, planning, and improving treatment.

## 2. Methods and Model

### 2.1 Problem statement

This study developed the 3D numerical modeling of the liver cancer treatment with the MWA process by using the single slot of microwave coaxial antenna (MCA). Slot coaxial antennas are common antennas in MWA application due to their advantages: size (small dimensions), design simplicity, low cost to manufacture, and convenient adaptation to treatment [28]. The single-slot MCA has a diameter of 1.79 mm; the antenna is required to be as small as possible for minimal invasiveness [9, 28]. A wide ring-shaped slot of 1 mm is cut off the outer conductor, and the length of 5.5 mm from the short-circuited tip to avoid the electric field from becoming stronger near the slot [33]. This antenna operated at the microwave power of 10 and frequency of 2.45 GHz for all cases of this study. The dimension and properties of single-slot MCA are shown in Table 1.

**Table 1.** Dimensions and dielectric properties of single slot MCA [1, 9, 28].

| Material | Dimensions (mm) | Dielectric properties | |
|---|---|---|---|
| | | Relative permittivity, $\varepsilon_r$ | Electric conductivity, $\sigma_{el}$ (S/m) |
| Inner conductor | 0.135 (radial) | - | - |
| Dielectric | 0.47 (radial) | 2.03 | 0 |

| | | | |
|---|---|---|---|
| Outer conductor | 0.595 (radial) | - | - |
| Catheter | 0.895 (radial) | 2.1 | 0 |
| Slot | 1.00 (wide) | 1 | 0 |

This study focused on the heat transfer in liver cancer during MWA treatment and thermal responses when the treatment area was close to a large blood vessel with a different locality. The comparison between the liver cancer embedded with vertical and horizontal large blood vessel models was investigated. In the first model, the model embedded with a vertical vessel has been assembled with four parts: 1) tumor domain, 2) healthy liver tissue domain, 3) MCA domain, and 4) a large blood vessel domain. The liver cancer model was considered to be the cube ( $80\times80\times80$ $mm^3$). The MCA was inserted on the top of the domain into the spherical tumor and parallel with the Y-axis. The center of the tumor and the slot were set to the insertion depth of 64 mm (Y-axis = 16 mm). The spherical tumor of 20 mm diameter was located on the center of the X and Z planes. A vertical blood vessel of 8 mm diameter [32] was located parallel with the MCA and 12 mm away from the MCA. The dimensions of the physical domain were based on literature [28, 32].

In the second model, the liver cancer embedded with a horizontal vessel model was assembled with four parts, the same as the model with a vertical vessel. The dimension of liver cancer with a horizontal vessel model was equally set to the vertical model, except for the vessel location. The center of the horizontal vessel was set at the same level as the center of the tumor. A horizontal blood vessel was located parallel with the X-axis. The distancing of the vessel wall to the center of the MCA was 12 mm, the same as the model with the vertical vessel. The physical properties of MCA, healthy liver tissue, tumor, and blood are shown in Table 2. This study investigated characteristic vessel locality on the SAR, temperature, and damaged tissue distribution in liver cancer during the MWA process. The system of the governing equations, as well as the initial condition and boundary condition, were solved numerically by using 3D FEM.

**Table 2.** The dielectric and thermal properties of the tissue [1, 9, 28].

| properties | Healthy liver tissue | Tumor | Blood |
|---|---|---|---|
| Relative permittivity, $\varepsilon_r$ | 43 | 48.16 | 58.3 |
| Electric conductivity, $\sigma_{el}$ (S/m) | 1.69 | 2.096 | 2.54 |
| Density, $\rho$ (kg/m$^3$) | 1030 | 1040 | 1058 |
| Thermal conductivity, $k_{th}$(W/m·ºC) | 0.497 | 0.57 | 0.45 |
| Specific heat capacity $C_p$ *(J/kg·ºC)* | 3,600 | 3,960 | 3,960 |

## 2.2 The electromagnetic wave propagation analysis

The electromagnetic wave propagation involved the performance of the MWA treatment. The governing equations and boundary conditions of electromagnetic wave propagation were considered in all domains. In order to simplify the problem, the assumptions are presumed as follows:

1. The electromagnetic wave propagation is propagated in three dimensions (3D) analysis.
2. The electromagnetic wave propagation in the MCA is characterized by transverse electromagnetic fields (TEM) [34].
3. The electromagnetic wave propagation in the biological tissue is characterized by transverse magnetic fields (TM) [34].
4. The model assumes that the dielectric properties of the liver are uniform and constant.

The propagation of the electromagnetic wave propagation in the antenna is by a transverse electromagnetic field (TEM) [1,3,9], given as:

Electric field $\left(\vec{E}\right)$

$$\vec{E} = e_r \frac{C}{r} e^{j(\omega t - kz)}. \quad (2.1)$$

Magnetic field $\left(\vec{H}\right)$

$$\vec{H} = e_\phi \frac{C}{rZ} e^{j(\omega t - kz)}, \quad (2.2)$$

where $C = \sqrt{\frac{ZP_{in}}{\pi \cdot \ln\left(R_{outer} / R_{inner}\right)}}$ is the arbitrary constant, $Z$ is the wave impedance $(\Omega)$, Pin is the microwave power input ($W$), $R_{outer}$ is the dielectric outer radius ($m$), $R_{inner}$ is the dielectric inner radius ($m$), $f$ is the frequency ($Hz$), $\omega = 2\pi f$ is the angular frequency (rad/s), k is the wave propagation constant ($m^{-1}$), which relates to the wavelength ($\lambda$) in medium: $k = \frac{2\pi}{\lambda}$.

The propagation of the electromagnetic wave in the biological tissue is by a transverse magnetic field (TM) as described by the following equation:

$$\nabla \times \left( \left( \frac{1}{\varepsilon_r} - \frac{j\sigma_{el}}{\omega \varepsilon_0} \right)^{-1} \nabla \times \vec{H}_\theta \right) - \mu_r k_0^2 \vec{H}_\theta = 0, \quad (2.3)$$

where $\vec{H}_\theta$ is magnetic field intensity ($A/m$), $\mu_r$ is relative permeability, $\varepsilon_r$ is relative permittivity, $\varepsilon_0 = 8.8542 \times 10^{-12}$ $F/m$ is permittivity of free space, $\sigma_{el}$ is electric conductivity ($S/m$), $k_0$ is the free space wavenumber ($m^{-1}$), and $\omega = 2\pi f$ is the angular frequency (rad/s).

The interaction of an electromagnetic wave with biological tissue could be defined in terms of *SAR* distribution. When the single-slot MCA transmits the electromagnetic wave, it passes through it and then propagates throughout the entire domain. The electromagnetic wave is absorbed and converted to internal heat in liver tissue. In this study, *SAR* represents the microwave power absorption deposited per unit mass in tissue ($W/kg$) [28]. The *SAR* is given by:

$$SAR = \frac{\sigma_{el}}{2\rho} \left| \vec{E} \right|, \quad (2.4)$$

where $\sigma_{el}$ is the electrical conductivity ($S/m$), $\rho$ is the tissue density ($kg/m^3$), and $\vec{E}$ is the electric field intensity ($V/m$). The *SAR* was converted to the heat generated in the biological tissue, which is defined as:

$$Q_{ext} = \frac{\sigma_{el} \left| \vec{E} \right|^2}{2} = \rho \cdot SAR. \quad (2.5)$$

The boundary conditions of electromagnetic wave propagation are applied for all domains. The electromagnetic wave boundary conditions of the model shown in Fig. 1, and the following conditions are made:

1. The outside of the computation domain is considered as a scattering boundary condition to eliminate the reflections:

$$\hat{n} \times \sqrt{\varepsilon} \vec{E} - \sqrt{\mu_{el}} \vec{H}_\theta = 2\sqrt{\mu_{el}} \vec{H}_{\theta 0}. \quad (2.6)$$

2. The interfaces between different mediums are considered as a continuity boundary condition:

$$\hat{n} \times \left( \vec{H}_1 - \vec{H}_2 \right) = 0. \quad (2.7)$$

3. The boundary conditions of the inner and outer conductor of MCA as the perfect electric conductor (PEC) boundary conditions:

$$\hat{n} \times \vec{E} = 0. \quad (2.8)$$

4. The port boundary condition is applied at the inlet of MCA with the microwave power set of 10 W.

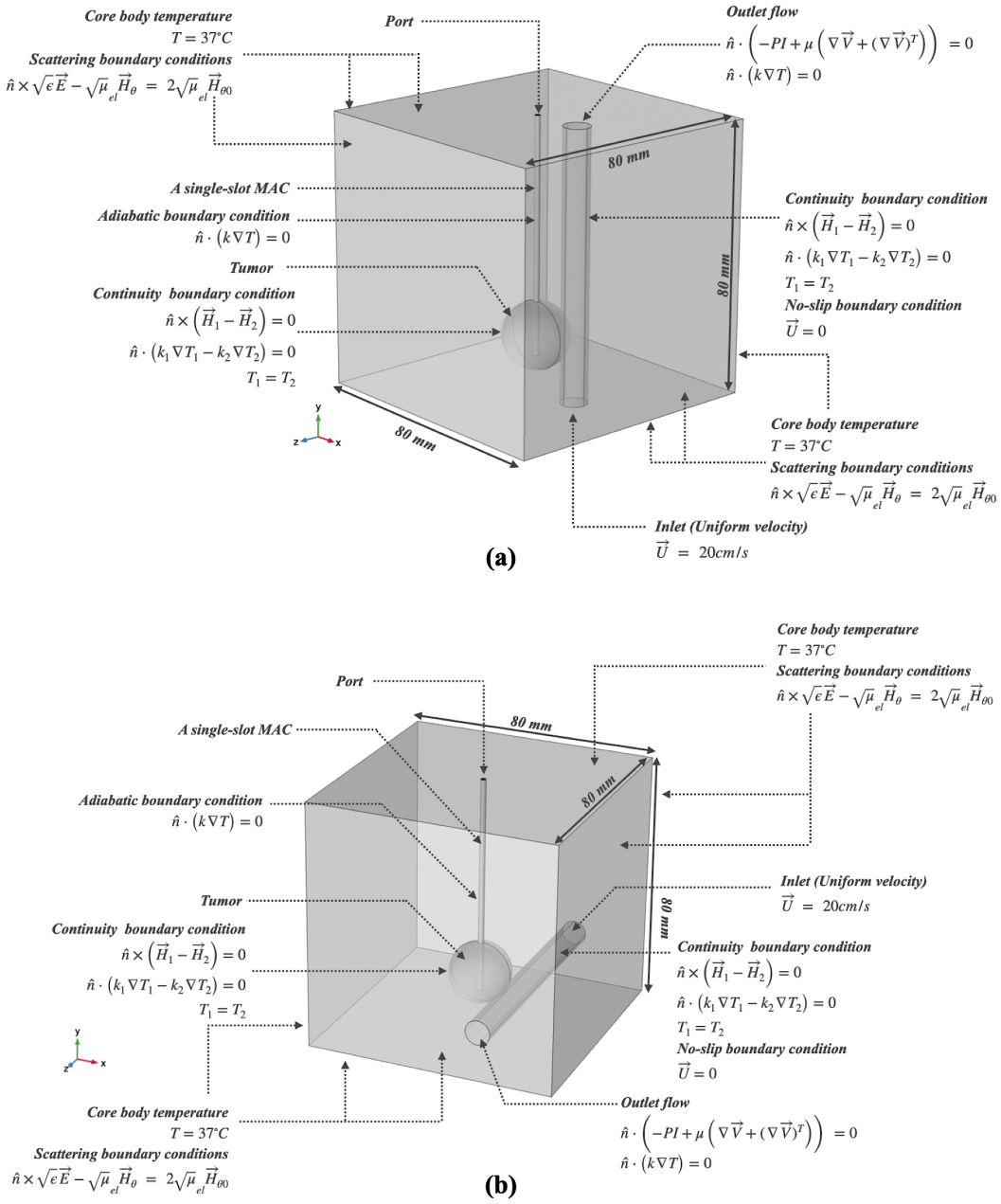


**Fig. 1.** The physical domain and boundary conditions of the liver cancer embedded with a large blood vessel model; (a) the model embedded with a vertical blood vessel, (b) the model embedded with a horizontal vessel.

### 2.3 Heat transfer in the biological tissue analysis

The heat transfer of biological tissue analysis is applied in the tumor and healthy liver tissue domains based on the bioheat equation. In this study, the biological tissue was the tumor and healthy liver tissue. For the reduced complexity of the problem, the heat transfer in the biological tissue follows these assumptions:

1. The heat transfer of the biological tissue based on the bioheat approach is considered in three- dimensional (3D) analysis.
2. The heat transfer of the biological tissue analysis is considered only in the tumor and healthy liver tissue.
3. The chemical reaction and phase change in the biological tissue are ignored.
4. The heat transfer of the single- slot MCA is ignored.
5. The healthy liver tissue and the tumor are assumed to be homogeneous and thermally isotropic.
6. The thermal properties of the biological tissue are uniform.

The heat transfer analysis of the biological tissue can be described by the Pennes bioheat equation [14], which can be written as follows:

$$\rho_t C_{p,t} \frac{\partial T}{\partial t} = \nabla \cdot k_{th,t} \nabla T + \rho_b C_{p,b} \omega_b \left(T_b - T\right) + Q_{met} + Q_{ext}, \tag{2.9}$$

where $\rho_t$ is the density of biological tissue ($kg/m^3$), $C_{p,t}$ is the specific heat capacity of tissue ($J/kg.$ ºC) , T is temperature of biological tissue (ºC), $k_{th,t}$ is the thermal conductivity of tissue ($W/m.$ºC), $\rho_b$ is the destiny of blood ($kg/m^3$), $C_{p,b}$ is the specific heat capacity of blood (J/kg.ºC), $\omega_b$ is blood perfusion rate ($s^{-1}$), $Q_{met}$ is the the metabolism heat source ($W/m^3$) and $Q_{ext}$ is the external heat source term ($W/m^3$). For liver carcinoma, the metabolism heat source is 4200 $W/m^3$, while the metabolism heat source in the healthy tissue is 42,000 $W/m^3$ [2, 40].

In the literature that concluded, the blood perfusion rate of tumors is lower than that in normal liver tissue. The blood perfusion rate of the normal liver tissue and the tumor is $6.4\times10^{-3}s^{-1}$ and $2.12\times10^{-3}s^{-1}$, respectively [32, 35]. Furthermore, the blood perfusion rate varies and is sensitive to the degree of tissue damage. Therefore, for accuracy, the calculation will consider the blood perfusion rate to the function of degrees of damage tissue, given as:

$$\begin{aligned}
&\omega_b(t) = \omega_{b0} && ;\Omega(t) \le 0 \\
&\omega_b(t) = \omega_{b0}\left[1 + 25\Omega(t) - 260(t)^2\right] && ;0 < \Omega(t) \le 0.1 \\
&\omega_b(t) = \omega_{b0}\exp\left[-\Omega(t)\right] && ;\Omega(t) \ge 0.1,
\end{aligned} \tag{2.10}$$

where $\omega_b$ is the blood perfusion rate of biological tissue. The $\omega_{b0}$ is the blood perfusion rate of biological tissue, and $\Omega(t)$ is the degree of tissue injury as shown in Eq. (22). The thermal conductivity of the biological tissue is also considered as a temperature dependent parameter, approximate as piecewise function [36].

$$\begin{aligned}
&k_{th}(T) = k_{ref} + 0.0013\left(T - T_{ref}\right) && ;T \le 100°C \\
&k_{th}(T) = k(100) && ;T \le 100°C.
\end{aligned} \tag{2.11}$$

The specific heat ($C_p$) of the biological tissue is considered piecewise function of temperature to liver cancer model. This function gives a constant value of $C_p$ when the temperature is below 63.5 ºC, but when the temperature is above 63.5 ºC, it gives a linear increasing function for $C_p$ [37].

$$\begin{aligned}
&C_p(T) = C_0 && ;T \le 63.5°C \\
&C_p(T) = C_0 + C_1\left(T - 63.5\right) && ;T \le 63.5°C,
\end{aligned} \tag{2.12}$$

where $C_0$ is the constant specific heat at temperature below 63.5 °C of the biological tissue and $C_1 = 28.9\ J/(kg{\cdot}K^2)$ [32]. For liver carcinoma, the specific heat reference is 3600 $J/kg{\cdot}$°C, while the specific heat

reference in the healthy tissue is 3960 $J/kg\cdot°C$.

The boundary conditions of heat transfer are applied in the biological domain. The heat transfer boundary conditions of the model are shown in Fig. 1 and the following conditions are made:

1. The interfaces between the biological tissue and the MCA are considered as the thermally insulated boundary condition:

$$\hat{n}\cdot\left(k\nabla T\right)=0. \tag{2.13}$$

2. The interfaces between the healthy liver tissue and the tumor are considered as the thermal continuity boundary conditions:

$$\hat{n}\cdot\left(k_1\nabla T_1-k_2\nabla T_2\right)=0, \tag{2.14a}$$

$$T_1=T_2. \tag{2.14b}$$

3. The surrounding of the healthy liver tissue domain is assumed to be the constant core body temperature:

$$T=37°C. \tag{2.15}$$

**2.3 Heat Transfer and blood flow analysis of a single blood vessel**

The heat transfer and blood flow analysis in this section is only considered in a large blood vessel. The governing equation and the boundary conditions are applied in the two models with the same condition. In order to simplify the problem, the assumptions are presumed as follows:

1. The heat transfer and blood flow of a single blood vessel are considered in three-dimensional (3D) analysis.
2. The blood is an incompressible and Newtonian fluid.
3. Chemical reaction of the countercurrent blood vessels is ignored.
4. The buoyancy effects of blood flow are neglected.
5. Fluid properties and thermal properties of in a large vessel are uniform and constant.

The heat convection can describe the heat convection of blood flow based on the energy equation, the equation of continuity, and the momentum equation, which can be written as follows:

Energy equation

$$\rho_b C_{p,b}\frac{\partial T_b}{\partial t}=\nabla\cdot k_b\nabla T_b+Q_{met}-\rho_b C_{p,b}\vec{U}\cdot\nabla T_b. \tag{2.16}$$

Momentum equation

$$\rho_b\left(\vec{U}\cdot\nabla\right)\vec{U}=-\nabla P+\mu_b\nabla^2\vec{U}. \tag{2.17}$$

Continuity equation

$$\nabla\cdot\left(\rho_b\vec{U}\right)=0, \tag{2.18}$$

where $\vec{U}$ is the velocity of blood ($m/s$), $\nabla P$ is the pressure gradient ($Pa$) and $\mu_b$ is the blood viscosity ($Pa.s$).

The boundary conditions of heat transfer and blood flow are applied for a blood vessel and shown in Fig. 1, and the following conditions are made:

1. The inlet flow of a single blood vessel is assumed to be uniform velocity [32, 38] and constant temperature as the core body temperature:

$$\vec{U}=20\ cm/s, \tag{2.19a}$$

$$T=37°C. \tag{2.19b}$$

2. The outlet flow of a single blood vessel is assumed to be outflow boundary condition:

$$\hat{n}\cdot\left(-PI+\mu\left(\nabla\vec{U}+\left(\nabla\vec{U}\right)^T\right)\right)=0, \tag{2.20a}$$

$$\hat{n}\cdot\left(k\nabla T\right)=0. \tag{2.20b}$$

3. The wall of a single blood vessel is considered as the thermal continuity boundary condition, and no-slip boundary condition:

$$\hat{n}\cdot\left(k_1\nabla T_1 - k_2\nabla T_2\right)=0, \quad (2.21a)$$

$$T_1 = T_2, \quad (2.21b)$$

$$\vec{U}=0. \quad (2.21c)$$

### 2.4 The damaged tissue analysis

The thermal damaged tissue analysis is applied in the healthy liver tissue and tumor (only the biological tissue). To simplify the problem, we considered the following assumptions:

1. The thermal damage of the biological tissue is considered in three- dimensional (3D) analysis.
2. The tissue damage analysis is only caused by thermal treatment.

Thermal damage is the thermal injury of biological tissue, for which the injury model proposed by Henriques & Moritz is used, namely the Arrhenius damage model [39]. The thermal damaged tissue can be defined as denaturation of the proteins in biological tissue, as follows:

$$\Omega(t) = A\int_0^t \exp\left(\frac{-E_a}{RT}\right)dt, \quad (2.22)$$

where $\Omega(t)$ is the cumulative tissue damage, $A$ is the frequency factor ($s^{-1}$), $E_a$ is the activation energy ($J/mol$) and R is the universal gas constant ($J/mol.K$). The fraction of necrotic tissue ($\theta_d$) can be expressed as:

$$\theta_d = 1-\exp\left(-\Omega(t)\right). \quad (2.23)$$

### 2.5 Initial condition

The initial electromagnetic field of the model was a set of 0 $V/m$. The initial temperature was set at the core temperature, 37 ºC. The microwave frequency was operating at 2.45 GHz and microwave power was 10 W for all cases.

## 3. Calculation procedure

In this study, the numerical procedure analyzes the liver cancer embedded with a single blood vessel model on the 3D transient problem. The computation model is coupled with the electromagnetic wave propagation, heat transfer in the biological tissue, and heat transfer in a single blood flow. The computation model is solved with FEM by using COMSOL™ Multiphysics, to demonstrate the effect of a vessel location on heat transfer phenomenon during the treatment process. The model is discretized using triangular elements with Lagrange quadratic shape functions, and the elements are adaptive in sensitive areas. The initial time- steps and the maximum time- steps to solve the transient problem are $1\times10^{-4}$ s and 0.1 s, respectively. The mesh independence test for the liver cancer model is shown in Fig. 2, which represents the temperature at a sensitive point. The density of elements, approximately 1,963,012 elements, meshes independently. Increasing the number of elements past this point did not lead to significantly different computational results.

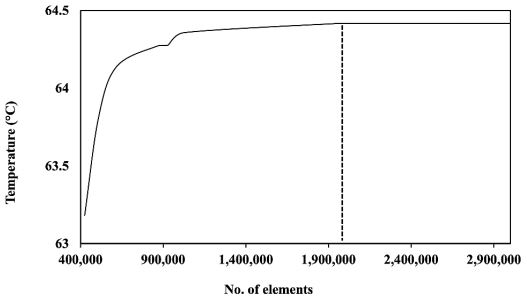


**Fig. 2.** Grid independence test.

## 4. Results and discussion

This work focused on different vessels located between the horizontal and vertical vessels on the SAR distribution, temperature distribution, blood flow, and damaged tissue in the liver cancer during the MWA treatment process. The coupled model of electromagnetic wave propagation, heat transfer in the biological tissue, and blood convection equations are solved numerically.

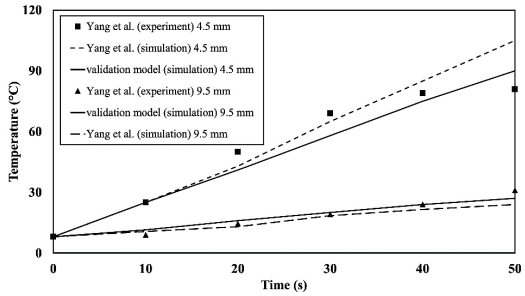


**Fig. 3.** The validation results of the calculated tissue temperature to the tissue temperature obtained by Yang et al. [21].

### 4.1 Verification of the model

In order to verify the model accuracy, the present numerical study was validated against the experimental results obtained by Yang et al. under the same testing conditions [21]. In the validation model, the MWA process operated with the microwave power input of 75 W with a frequency of 2.45 GHz, and the initial temperature was set at 8°C. The MWA using a slot MCA had a radius of 1.25 mm. The MCA was inserted 20 mm deep into the biological tissue with a heating time of 50 s. The verification results show the transient temperature of two points, which are 4.5 and 9.5 mm away from the MCA, as shown in Fig. 3. Table 3 shows a comparison of RMSE values between the present model and the analytical study obtained by Yang et al. [3, 21]. The verification results were clearly in good agreement with the experimental results and gave confidence in the accuracy of the presented numerical models.

**Table 3.** Comparisons of RMSE of the liver tissue temperature between the presented model and Yang et al. [3, 21].

| Position (mm) | Comparisons of RMSE with experiment from Yang et al., (ºC) | |
|---|---|---|
| | Presented study (Brinkman) | Yang et al. (simulation model) |
| 4.5 | 3.95 | 11.03 (Keangin et al., 2011) |
| 9.5 | 3.50 | 5.57 (Keangin et al., 2011) |

### 4.2 The electromagnetic wave propagation analysis

The basic principle of the MWA treatment is to apply microwave energy into the tumor. The microwave energy is transmitted by using MCA. The microwave energy is absorbed and converted to the internal heat generation in the tumor. This treatment aims to create damage in the tumor by using thermal energy from the microwave source. The SAR distribution is one of the most important factors affecting the effectiveness of the treatment [28]. In this study, the liver cancer model embedded with a large blood vessel used single-slot MCA for treatment. The MCA operated on the microwave frequency of 2.45 GHz and microwave power of 10 W for all cases. The electromagnetic wave propagation between the model with the vertical and horizontal vessels was compared and represented on the SAR distribution on the cross-section plane, as shown in Fig. 4. This plane was a cross-section at the center of the model, which went through the tumor and a blood vessel.

Fig. 4 shows the SAR intensity distribution exhibit similar to a water droplet. The highest value of SAR appealed to the slot area and decreased with the distance away from the slot. In the tumor area, the SAR distribution is higher than the area of the healthy liver tissue. Fig. 5 shows the SAR profile with the insertion depth line between the model with the vertical and horizontal vessel at the heating time of 10 min. The insertion depth line is parallel to the MCA and away from the MCA centerline of 2.5 mm. The SAR maximum appeared in the slot area and decreased with distance away from the slot, which corresponded with the 2D SAR distribution. The value of SAR between the model with a vertical vessel and the horizontal vessel were similarly distributed. This is because the models used an MCA and the dielectric properties of materials with the same treatment conditions. Furthermore, the location of a large vessel was far away from the SAR distribution intensive area.

Therefore, the location characteristic of a single vessel has not affected the SAR distribution between the models with the vertical and horizontal vessel.

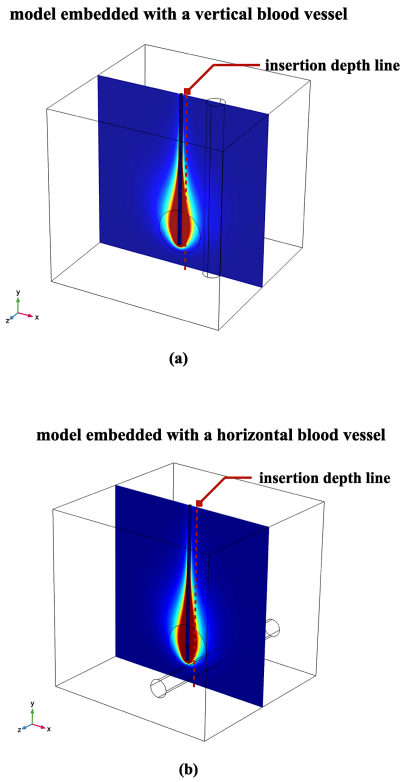


**Fig. 4.** The SAR distribution at the cross-section plane with microwave power of 10 W, and frequency of 2.45 GHz; (a) the model embedded with a vertical vessel, (b) the model embedded with a horizontal vessel.

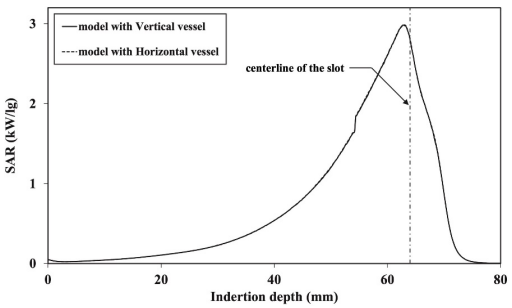


**Fig. 5.** SAR profile at the insertion depth line between the model embedded with a vertical and horizontal vessel with microwave power of 10 W, and frequency of 2.45 GHz.

## 4.2 Heat transfer analysis

The temperature distribution in the liver cancer model during the MWA treatment process is related to the performance of this treatment. In this study, the volumetric heating effect on the biological tissue is induced by microwave energy. The MCA transmits the microwave energy into the tumor area. The microwave energy is absorbed and converted to internal heating in the biological tissue domain. In order to study the heat transfer in the model, the coupled effects of the electromagnetic wave propagation, heat transfer, and blood flow in a large vessel flow are considered.

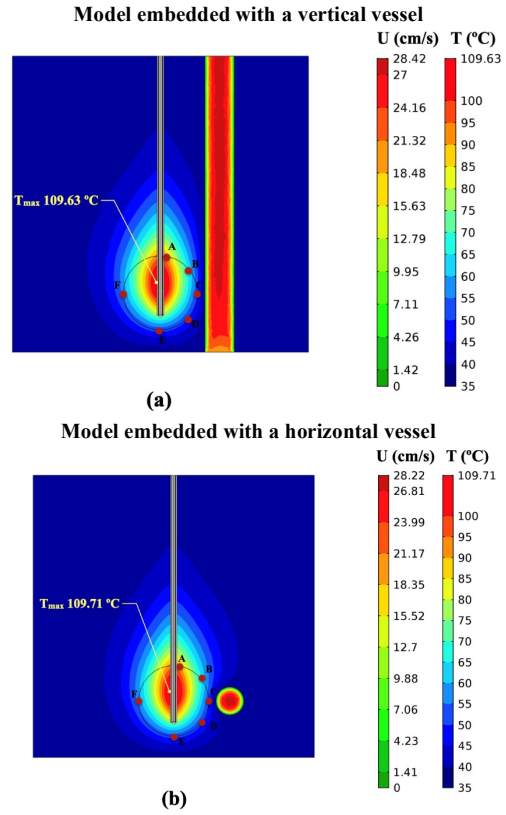


**Fig. 6.** Temperature and velocity fields at the cross-section plane with microwave power of 10 W, frequency of 2.45 GHz, and heating time of 10 min; (a) the model with a vertical vessel, (b) the model with a horizontal vessel.

Fig. 6 shows the temperature and blood velocity distribution in the cross-section plane of the 3D liver cancer model during the MWA process at the heating time of 10 min, Fig. 6( a) is the model with a vertical vessel, and Fig. 6( b) is the model with a horizontal vessel. The temperature intensity occurred in the slot area and decreased with distance away from the slot. This result corresponded with the SAR distribution ( shown in Fig. 4) because SAR in the biological tissue owned the energy absorption. After that, the microwave energy absorption is converted to thermal energy, which leads to increased temperature in the biological tissue.

The intensity temperature distribution exhibit, similar to a droplet of water, corresponds to the SAR distribution. However, the temperature distribution around the area of blood vessel flow is different. The different points between the model with a vertical and horizontal vessel could be observed on the low- temperature contour at the area close to a single blood vessel. In this area, the heat transfer phenomenon plays the role of blood convection by a single vessel. The maximum temperature on the cross-section plane of the model with a vertical and horizontal vessel is 109.63 ºC and 109.71 ºC, respectively. Although a vertical and horizontal blood vessel was equally uniform inlet velocity and vessel length, the temperature distributions differed. The temperature distribution indicated that the heat transfer by a vertical blood vessel was higher than a horizontal blood vessel

Fig. 7 shows the transient temperature of the model with a vertical and horizontal vessel on the selected points. The selected points were set around the tumor boundary. For all points, the temperature increases with the heating time. The temperature of point *A* was highest, followed by points *B*, *F*, *E*, *D*, and *C*, respectively. The temperature difference between the two models can be clearly observed at point *B*. Fig. 8 shows the transient temperature difference of point *A* to *F* between the model with a horizontal vessel and a vertical vessel. In this result, the method is to take the temperature at the same point of the horizontal vessel model minus the vertical vessel model. The temperature difference of point *B* had the highest value, followed by points *A*, *D*, *C*, *E*, and *F*, respectively. The transient temperature of point *A* was the highest value, but the temperature difference between the two models was not dependent on the high temperature. At point *C*, that position closest to a large vessel, the temperature difference between the two models was not clearly observed. The highest temperature difference is shown on point *B*, in which the area was not the highest temperature increasing and not closest to a blood vessel. The heat transfer between the heat sink and source relates to the surface area and the distancing between the heat sink and source in the heat transfer mechanism. The temperature difference of point *B* was caused by the factor of surface area and the distancing between the heat sink and the heat source. In this case, the heat source was the high temperature in the tumor, and the heat sink was the blood flow in a vessel. This result was affected by the temperature distribution, which induced the heat transfer by a vertical blood vessel that was higher than the heat transfer by a horizontal blood vessel.

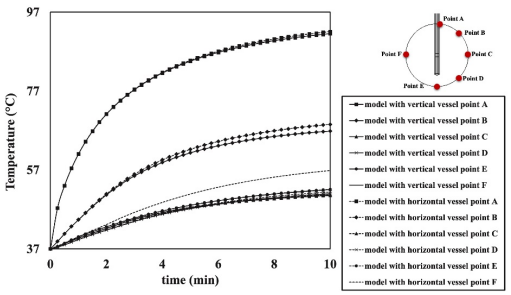


**Fig. 7.** The comparison of the transient temperature at the selected points between model with a vertical and horizontal vessel with microwave power of 10 W, frequency of 2. 45 GHz.

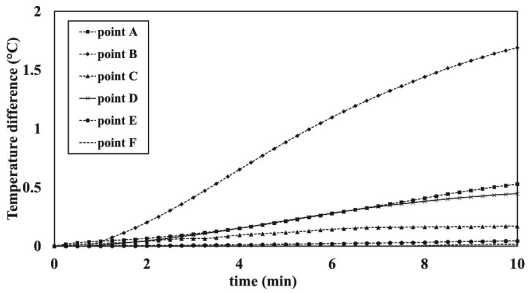


**Fig. 8.** The transient temperature difference of the selected points between model with a horizontal and vertical vessel with microwave power of 10 W, and frequency of 2.45 GHz.

The microwave energy was transmitted by a single slot MCA into the tumor and healthy liver tissue. The microwave energy is absorbed and converted to heat by dielectric heating. The microwave energy absorbed was intensely distributed on the slot area and decreased with the distance away from the slot. The temperature distribution was similarly distributed to the SAR distribution. Because the energy absorbed by the microwave was converted to thermal energy, leading to increased temperature in this biological tissue. A single vertical and horizontal vessel was embedded in the area closed to the treatment area. The heat transfer in this area was conjugated between heat conduction and heat convection. However, the vertical blood vessel was transferred heat energy more than the horizontal vessel. The heat pattern in this model was influenced by the surface and distancing between the hot spot as well as the heat source to the heat sink, which was a blood vessel.

### 4.3 Damaged tissue analysis

This treatment aimed to create the fully damaged only tumor area and without damage to the healthy liver tissue area. In this study, the tissue damage was only affected by thermal energy and considered only the biological domain. The thermal damage model was investigated based on the Arrhenius damage model. The fraction of damaged tissue increases with the degree of thermal denaturation (percentage of denatured collagen), where $\theta_d = 0$ indicates no damage in the liver tissue. In contrast, $\theta_d = 1$ indicates fully damaged liver tissue. Fig. 9 shows the fraction of the damaged tissue and blood velocity vector on the cross-section plane during the MWA process at the heating time of 10 min; Fig. 9(a) the model with a vertical vessel, and Fig. 9(b) the model with a horizontal vessel. The fully damaged tissue occurred in the tumor area and upper of the tumor. The shape of the damaged tissue was similar to a droplet of water, which corresponded with SAR and temperature distribution.

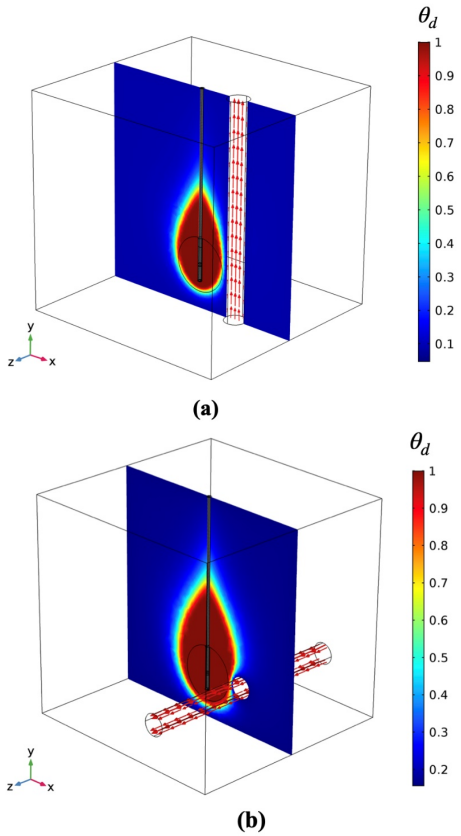


**Fig. 9.** The fraction of damaged tissue distribution and velocity arrow at the cross-section plane with microwave power of 10 W, frequency of 2.45 GHz, and heating time of 10 min; (a) the model with a vertical vessel, (b) the model with a horizontal vessel.

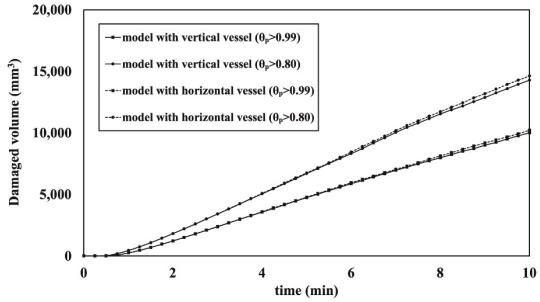


**Fig. 10.** The comparison volumetric of damaged tissue between the model with a vertical and horizontal vessel, with microwave power of 10 W, frequency of 2.45 GHz.

The volumetric of fully damaged between the model with vertical and horizontal was slightly different. The fully damaged tissue occurred in the hot spot area, which was slightly affected by the characteristic of blood vessel location. However, the volumetric damaged tissue faction above 0.80 shows a clear difference between the two models. This volumetric included the volume of biological tissue wider than the boundaries tumor, which included the area close to a large blood vessel locality. Therefore, the effect of a blood vessel locality clearly occurred. Finally, the damaged tissue analysis on this biological tissue depended on the temperature distribution, which was owed to the microwave power absorbed.

## 5. Conclusion

This study developed the 3D numerical model of the liver cancer embedded with a large vessel flow during MWA treatment by using the MCA. The influence of a blood vessel locality was investigated. Comparison between the model embedded with a vertical blood vessel and a horizontal blood vessel was represented on the SAR distribution, temperature distribution, and damaged tissue contour in the liver cancer tissue. The mathematical modeling was considered coupled with the electromagnetic wave propagation, heat transfer, and blood flow equations. The system of the governing equations, as well as the initial condition and boundary condition, were solved numerically by using 3D FEM. The electromagnetic wave propagation was expressed mathematically by Maxwell' s equations. The heat transfer model was developed based on the bioheat equation in the biological tissue domain and the energy conservation equation of the fluid (blood) flow. Furthermore, the blood flow analysis was expressed mathematically by the momentum and continuity equations. The damaged tissue model was developed based on the Arrhenius damage model.

To verify the model accuracy, the model was validated against the experimental results obtained by Yang et al. under the same testing conditions. The comparison between the liver cancer embedded with a vertical vessel and a horizontal vessel during MWA treatment was investigated under the same boundary and initial conditions. The effect of blood vessel locality on liver cancer during the MWA treatment was presented on the SAR distribution, temperature distribution, and damaged tissue. The SAR between the model embedded a vertical vessel and a horizontal vessel were similarly distributed. Because the blood vessel was located far away from the slot area, which SAR distributed intensively, the different locality of a large vessel could not annoy SAR distribution, especially in high-SAR-intensity areas. However, the temperature distribution between the embedded a vertical vessel and a horizontal vessel were clearly different in the area near a large blood vessel. Moreover, the temperature at the tumor boundary was influenced by the effect of a blood vessel locality. The simulation results indicated that the temperature distribution at the tumor boundary of the model embedded with a horizontal vessel was higher than the model embedded with a vertical vessel. That is caused by the surface area and the distancing between the heat sink and the heat source. In this case, the heat source was the high

temperature in the tumor, and the heat sink was the blood flow in a vessel. This result was affected by the temperature distribution, which induced the heat transfer by a vertical blood vessel that was higher than the heat transfer by a horizontal blood vessel. In damaged tissue analysis, the fully damaged tissue between the model embedded with a vertical vessel and a horizontal vessel were similar. Furthermore, the highly damaged tissue between the model embedded with a vertical vessel and a horizontal vessel has demonstrated the effect of a large blood locality, which corresponds with the temperature distribution.

In addition, when a large blood vessel would be considered with different sides of the tumor under the same conditions and distancing should demonstrate similar results. Due to results as well as SAR distribution, temperature distribution, and damaged tissue in the liver cancer model during MWA treatment were axisymmetric distributed when did not include flow in the large blood vessel analysis. As a result, the cases will be considered a large blood vessel on opposite sides of the tumor under the same conditions should demonstrate similar results. However, when taking the place of treatment near the large vessel with MWA, the simulation results demonstrated the asymmetry of the temperature distribution and damaged tissue distribution during the MWA treatment process. Accordingly, the heat transfer analysis should be considered under the 3D assumption.

In this study, the microwave power absorbed in liver cancer was owning to the energy absorption. After that, the energy absorption was converted to thermal energy, leading to increased biological tissue temperature and damaged tissue volumetric. A large blood vessel nearby the treatment area affected the heat transfer in the treatment area, which related to the effective performance of the treatment process. Therefore, this study presented SAR distribution, temperature distribution, and damaged tissue in liver cancer embedded with a large vessel during MWA treatment with the symmetrical investigation. The simulation results in this study can be used as a guideline concerning the effect of blood vessel locality near the treatment area during the MWA process.

## Acknowledgements

The authors gratefully acknowledge the Thailand Science Research and Innovation (under the Royal Golden Jubilee Ph. D. Program (RGJ) contract No. PHD/0055/2558) and PMU B (Contract No. B05F630092) provided financial support for this study.

## References

[1] Keangin P, Rattanadecho P, Wessapan T. An analysis of heat transfer in liver tissue during microwave ablation using single and double slot antenna. International Communications in Heat and Mass Transfer. 2011 Jul 1;38(6):757-66.

[2] Nabaei M, Karimi M. Numerical investigation of the effect of vessel size and distance on the cryosurgery of an adjacent tumor. Journal of thermal biology. 2018 Oct 1;77:45-54.

[3] Keangin P, Wessapan T, Rattanadecho P. Analysis of heat transfer in deformed liver cancer modeling treated using a microwave coaxial antenna. Applied Thermal Engineering. 2011 Nov 1;31(16): 3243-54.

[4] Dong BW, Liang P, Yu XL, Zeng XQ, Wang PJ, Su L, Wang XD, Xin HO, Li SO. Sonographically guided microwave coagulation treatment of liver cancer: an experimental and clinical study. AJR. American journal of roentgenology. 1998 Aug;171(2):449-54.

[5] Goldberg SN, Gazelle GS, Mueller PR. Thermal ablation therapy for focal malignancy: a unified approach to underlying principles, techniques, and diagnostic imaging guidance. American

journal of roentgenology. 2000 Feb;174(2):323-31.

[6] Whelan WM, Davidson SR, Chin LC, Vitkin IA. A novel strategy for monitoring laser thermal therapy based on changes in optothermal properties of heated tissues. International Journal of Thermophysics. 2005 Jan 1;26(1):233-41.

[7] Prakash P, Deng G, Converse MC, Webster JG, Mahvi DM, Ferris MC. Design optimization of a robust sleeve antenna for hepatic microwave ablation. Physics in Medicine & Biology. 2008 Jan 28;53(4):1057.

[8] Wang T, Zhao G, Qiu B. Theoretical evaluation of the treatment effectiveness of a novel coaxial multi-slot antenna for conformal microwave ablation of tumors. International Journal of Heat and Mass Transfer. 2015 Nov 1;90:81-91.

[9] Keangin P, Rattanadecho P. Analysis of heat transport on local thermal non-equilibrium in porous liver during microwave ablation. International Journal of Heat and Mass Transfer. 2013 Dec 1;67:46-60.

[10] Lopresto V, Pinto R, Farina L, Cavagnaro M. Microwave thermal ablation: effects of tissue properties variations on predictive models for treatment planning. Medical engineering & physics. 2017 Aug 1;46: 63-70.

[11] Hines- Peralta AU, Pirani N, Clegg P, Cronin N, Ryan TP, Liu Z, Goldberg SN. Microwave ablation: results with a 2.45-GHz applicator in ex vivo bovine and in vivo porcine liver. Radiology. 2006 Apr;239(1):94-102.

[12] Strickland AD, Clegg PJ, Cronin NJ, Swift B, Festing M, West KP, Robertson GS, Lloyd DM. Experimental study of large-volume microwave ablation in the liver. British Journal of Surgery. 2002 Aug 1;89(8):1003-7.

[13] Marcelin C, Leiner J, Nasri S, Petitpierre F, Le Bras Y, Yacoub M, Grenier N, Bernhard JC, Cornelis F. In vivo percutaneous microwave ablation in kidneys: Correlation with ex vivo data and ablation work. Diagnostic and interventional imaging. 2018 Jan 1;99(1):3-8.

[14] Pennes HH. Analysis of tissue and arterial blood temperatures in the resting human forearm. Journal of applied physiology. 1998 Aug 1;1(2):93-122.

[15] Wulff W. The energy conservation equation for living tissue. IEEE transactions on biomedical engineering. 1974 Nov(6):494-5.

[16] Klinger HG. Heat transfer in perfused biological tissue— I: General theory. Bulletin of Mathematical Biology. 1974 Feb 1;36:403-15.

[17] Chen MM, Holmes KR. Microvascular contributions in tissue heat transfer. Annals of the New York Academy of Sciences. 1980 Mar;335(1):137-50.

[18] Keller KH, Seiler Jr LO. An analysis of peripheral heat transfer in man. Journal of Applied Physiology,. 1971 May;30(5):779-86.

[19] Weinbaum SJ, Jiji LM, Lemons DE. Theory and experiment for the effect of vascular microstructure on surface tissue heat transfer— Part I: Anatomical foundation and model conceptualization.

[20] Jiji LM, Weinbaum S, Lemons DE. Theory and experiment for the effect of vascular microstructure on surface tissue heat transfer—part II: model formulation and solution.

[21] Yang D, Converse MC, Mahvi DM, Webster JG. Expanding the bioheat equation to include tissue internal water evaporation during heating. IEEE Transactions on Biomedical Engineering. 2007 Jul 16;54(8):1382-8.

[22] Wu X, Liu B, Xu B. Theoretical evaluation of high frequency microwave ablation applied in cancer therapy. Applied Thermal Engineering. 2016 Aug 25;107:501-7.

[23] Xu Y., Moser M. A., Zhang E., Zhang W., Zhang B. Large and round ablation zones with microwave ablation: A preliminary study of an optimal aperiodic tri- slot coaxial antenna with the π- matching network section. International Journal of Thermal Sciences. 2019;140:539-48.

[24] Soltani M., Tehrani M. H., Kashkooli F. M., Rezaeian M. Effects of magnetic nanoparticle diffusion on microwave ablation treatment: A numerical approach. Journal of Magnetism and Magnetic Materials. 2020;514:167196.

[25] Khaled AR, Vafai K. The role of porous media in modeling flow and heat transfer in biological tissues. International Journal of Heat and Mass Transfer. 2003 Dec 1;46(26):4989-5003.

[26] Khanafer K, Vafai K. The role of porous media in biomedical engineering as related to magnetic resonance imaging and drug delivery. Heat and mass transfer. 2006 Aug;42(10):939-53.

[27] Nakayama A, Kuwahara F. A general bioheat transfer model based on the theory of porous media. International Journal of Heat and Mass Transfer. 2008 Jun 1;51(11-12):3190-9.

[28] Rattanadecho P, Keangin P. Numerical study of heat transfer and blood flow in two- layered porous liver tissue during microwave ablation process using single and double slot antenna. International Journal of Heat and Mass Transfer. 2013 Mar 1;58(1-2):457-70.

[29] Pongpakpien S., Preechaphonkul W., Rattanadecho P. Effects of thermal and electrical properties on porous liver during microwave ablation using microwave coaxial slot antenna. Int J Heat Technol. 2019;38(2):361-70.

[30] Preechaphonkul W, Rattanadecho P. The comparative of the performance for predicted thermal models during microwave ablation process using a slot antenna. Case Studies in Thermal Engineering. 2021;25:100908.

[31] Zorbas G, Samaras T. A study of the sink effect by blood vessels in radiofrequency ablation. Computers in biology and medicine. 2015 Feb 1;57:182-6.

[32] Shao YL, Arjun B, Leo HL, Chua KJ. Nano- assisted radiofrequency ablation of clinically extracted irregularly- shaped liver tumors. Journal of thermal biology. 2017 May 1;66:101-13.

[33] Saito K, Hayashi Y, Yoshimura H, Ito K. Heating characteristics of array applicator composed of two coaxial-slot antennas for microwave coagulation therapy. IEEE Transactions on Microwave Theory and Techniques. 2000 Nov;48(11):1800-6.

[34] Bertram JM, Yang D, Converse MC, Webster JG, Mahvi DM. Antenna design for microwave hepatic ablation using an axisymmetric electromagnetic model. Biomedical engineering online. 2006 Dec;5(1):1-9.

[35] Jain RK. Determinants of tumor blood flow: a review. Cancer research. 1988 May 15;48(10):2641-58.

[36] Trujillo M, Berjano E. Review of the mathematical functions used to model the temperature dependence of electrical and thermal conductivities of biological tissue in radiofrequency ablation. International Journal of Hyperthermia. 2013 Sep 1;29(6):590-7.

[37] Dos Santos I, Haemmerich D, Schutt D, da Rocha AF, Menezes LR. Probabilistic finite element analysis of radiofrequency liver ablation using the unscented transform. Physics in Medicine & Biology. 2009 Jan 6;54(3):627.

[38] Lee ES, Lee JM, Kim WS, Choi SH, Joo I, Kim M, You DH, You RE, Han JK, Choi BI. Multiple- electrode radiofrequency ablations using Octopus® electrodes in an in vivo porcine liver model. The British journal of radiology. 2012 Sep;85(1017):e609-15.

[39] Moritz AR, Henriques Jr FC. Studies of thermal injury: II. The relative importance of time and surface temperature in the causation of cutaneous burns. The American journal of pathology. 1947 Sep;23(5):695.

[40] Deng Z. S., Liu J. Numerical simulation of selective freezing of target biological tissues following injection of solutions with specific thermal properties. Cryobiology. 2005;50(2):183-92.

[41] Gheflati B. , Naghavi N. Computational study of nanoparticle assisted hyperthermia in tumors embedded with large blood vessels. International Journal of Heat and Mass Transfer. 2020;151:119415.